UCRL-ID-111564

PCMDI Report No. 4

BEHAVIOR OF AN OCEAN GENERAL CIRCULATION MODEL AT FOUR DIFFERENT HORIZONTAL RESOLUTIONS

by

Curt Covey

Program for Climate Model Diagnosis and Intercomparison
Lawrence Livermore National Laboratory
Livermore, CA, USA

August 1992

PROGRAM FOR CLIMATE MODEL DIAGNOSIS AND INTERCOMPARISON
UNIVERSITY OF CALIFORNIA, LAWRENCE LIVERMORE NATIONAL LABORATORY
LIVERMORE, CA 94550

ABSTRACT

A global ocean general circulation model is used to simulate the present-day ocean climate using four different latitude / longitude grid spacings. Horizontal resolution varies from 1/2° x 1/2° —the highest attained to date in an ocean circulation model with global coverage—to a coarse 4° x 4° grid traditionally used in climate modelling. This study addresses the question of whether resolution of smaller-scale circulations is necessary in order to simulate the large-scale ocean climate correctly. Results indicate that large-scale circulation is rather sluggish at 4° x 4° resolution but surprisingly insensitive to grid spacing for resolutions better than 2° x 2°, even considering the constraints imposed on the model by surface boundary conditions and by "robust diagnostic" forcing near the poles and below the thermocline. Simulated transport of heat from the warm tropics to cooler higher latitudes is not overly sensitive to grid spacing for resolutions better than 2° x 2°. Furthermore, heat transport does not increase at 1/2° x 1/2° resolution when sub-gridscale mixing of heat and momentum are altered so that mesoscale eddies appear in the model.

These results support inferences from earlier studies (based on simplified, limited-domain circulation models) that mesoscale eddies make little net contribution to poleward heat transport by the oceans. They suggest that for global climate modeling, the substantial computer resources required to explicitly resolve ocean mesoscale eddies might be better spent on improving simulations of other components of the climate system. Making this conclusion definite, however, requires a global ocean simulation that is fully eddy-resolving and that relaxes the artificial constraints of the present simulation, which tend to force the results toward present ocean climatology.

1. Introduction

This report describes how an ocean general circulation model (OGCM) behaves as a function of horizontal resolution. The study was undertaken at LLNL as part of the Program for Climate Model Diagnosis and Intercomparsion, in parallel with a PCMDI study of the behavior of an atmospheric GCM as a function of horizontal resolution (Gates et al., 1992).

One motive for this study is provided by the fact that most of the kinetic energy of ocean currents is observed at horizontal scales less than ~100 km (see, e.g., Figure 6 of Woods, 1985). In the atmosphere, the kinetic energy spectrum peaks at several thousand kilometers, the scale of baroclinic waves. Analogous waves in the ocean—the so-called mesoscale eddies—have a size of only ~50 km. Coupled ocean-atmosphere general circulation models, which are often used to estimate global warming due to human-produced greenhouse gases, typically operate with horizontal grid-point spacings of several hundred kilometers. Such models are unable to resolve the ocean's mesoscale eddies. The question naturally arises whether mesoscale eddies in the ocean transport a significant amount of heat from the warm tropics to the cooler polar regions, as do baroclinic waves in the atmosphere. If so, then OGCMs intended for climate purposes would need to incorporate a successful parameterization of mesoscale eddies, or to explicitly resolve the mesoscale eddies, a formidable imposition on computer resources.

A second and more immediate objective of this study is simply to assess how much one gains by paying the computer-time cost of enhancing resolution. Theoretically each factor-of-two reduction in horizontal grid spacing requires a factor of eight more computer time: two factors of two from the horizontal dimensions and an additional factor of two from the need to reduce the time step. Actually the computer time increases somewhat less rapidly (a factor between five and six for halved grid spacing in the work reported here), but the cost-versus-resolution curve is quite steep. For a climate simulation, in which the ocean model would be linked with models of other components of the Earth System, one may well reach a point of diminishing returns where the cost of enhancing an OGCM's horizontal resolution would be better spent elsewhere.

Several OGCM studies have approached the question of whether horizontal resolution limits the simulation of large-scale climate. Results to date—which

include model resolutions as fine as 1/6° latitude—suggest that large-scale features of the simulations are not particularly sensitive to resolution, and that mesoscale eddies do not transport significant amounts of heat (Bryan, 1991). These studies, however, are incomplete in two ways. First, in order to conserve computer time, the models were run over a limited domain with unrealistic "box-like" geometry. Second, the models did not separate temperature and salinity effects. The models used a single equation, expressing conservation of potential density, in place of two separate equations that would express conservation of thermal energy and salt. Strictly speaking, the "heat" transport simulated by these models is actually transport of bouyancy. As Bryan (1986) points out, "Heat transport may take place by eddies in the real ocean without eddy bouyancy transport, since temperature gradients always exist on isopycnal surfaces and may be quite strong in polar regions." The work described in this report removes both constraints of previous studies, i.e., it employs an OGCM with realistic global geography and bottom topography, and with separate treatment of heat and salt transport.

2. The model

The model chosen for this study is the OGCM described by Semtner and Chervin (1988). Traditionally, OGCMs come in two varieties: high resolution / limited domain and low resolution/global domain. The Semtner-Chervin model evolved from the latter category. As described by Semtner and Chervin, however, it has recently been run at latitude/longitude grid spacing of 1/2° x 1/2°. This resolution is the highest achieved to date by an OGCM with global coverage. In this study I compare simulations at 1/2° x 1/2° with simulations at three lower resolutions: 1° x 1°, 2° x 2° and 4° x 4° (vertical resolution is held constant at 20 levels). A 4° x 4° horizontal resolution is typical of global-domain OGCMs that are used together with atmospheric GCMs to simulate global warming due to human production of greenhouse gases (e.g., Washington and Meehl, 1989; Manabe et al., 1990).

Two earlier studies have examined the behavior of Semtner and Chervin's 20-level model as a function of resolution. Barton (1988) compares 1° x 1° and 1/2° x 1/2° resolutions, although the amount of "robust-diagnostic" forcing (see below) differs in his two cases. Washington et al. (1992) report the effects of degrading reso-

lution from 1/2° x 1/2° to 1° x 1°, and at the same time adding the Arctic Ocean and a sub-model of sea ice. Although these studies involved changes in more than just resolution, they provided a valuable guide for my work.

All GCMs—including even the high resolution, limited-domain OGCMs mentioned above—must account for scales of circulation smaller than the spacing of their grid points by means of "sub-gridscale parameterizations." Chief among these parameterizations are formulas for the mixing of momentum and heat at small scales. Semtner and Chervin (1988) take a traditional approach to sub-gridscale horizontal mixing, parameterizing it as down-gradient diffusion with a constant coefficient. In their 1/2° x 1/2° experiments, two forms of sub-gridscale horizontal diffusion were used: Laplacian (rate of change due to diffusion is proportional to the second derivative of concentration) and biharmonic (rate of change is proportional to the fourth derivative of concentration). Semtner and Chervin (1988) show that use of the more scale-selective biharmonic diffusion parameterization allows resolution of some mesoscale eddies at 1/2° x 1/2° resolution. In the experiments conducted at LLNL, only the Laplacian form of diffusion was used. Later in this report, however, results from the LLNL experiments are compared with Semtner and Chervin's biharmonic-diffusion results.

One consequence of sub-gridscale parameterizations in GCMs is that changing only the resolution in such models is impossible. As distance between grid points is increased, the amount of sub-gridscale mixing needs to be increased; otherwise the computation becomes numerically unstable. Figure 1 shows the combination of horizontal resolution and horizontal momentum diffusion (or viscosity) coefficients used in this study and in examples of other OGCM work. The latter include the pioneering eddy-resolving model of Holland and Lin (1975a,b), the pioneering global-scale model of Bryan et al. (1975) and a more recent global scale model (Washington and Meehl, 1989). The figure shows that the Semtner-Chervin model, with the different resolutions examined in this study, largely spans the gap between the high resolution / limited domain and low resolution / global domain varieties of OGCMs.

At 1/2° x 1/2° resolution I followed Semtner and Chervin (1988) in using identical diffusion coefficients of 10^3 m^2 s^{-1} for both momentum and heat. These coefficients were increased linearly with grid-point spacing at 1° x 1° and 2° x 2° resolution. At 4° x 4° resolution, I used a heat diffusion scaled with grid-point

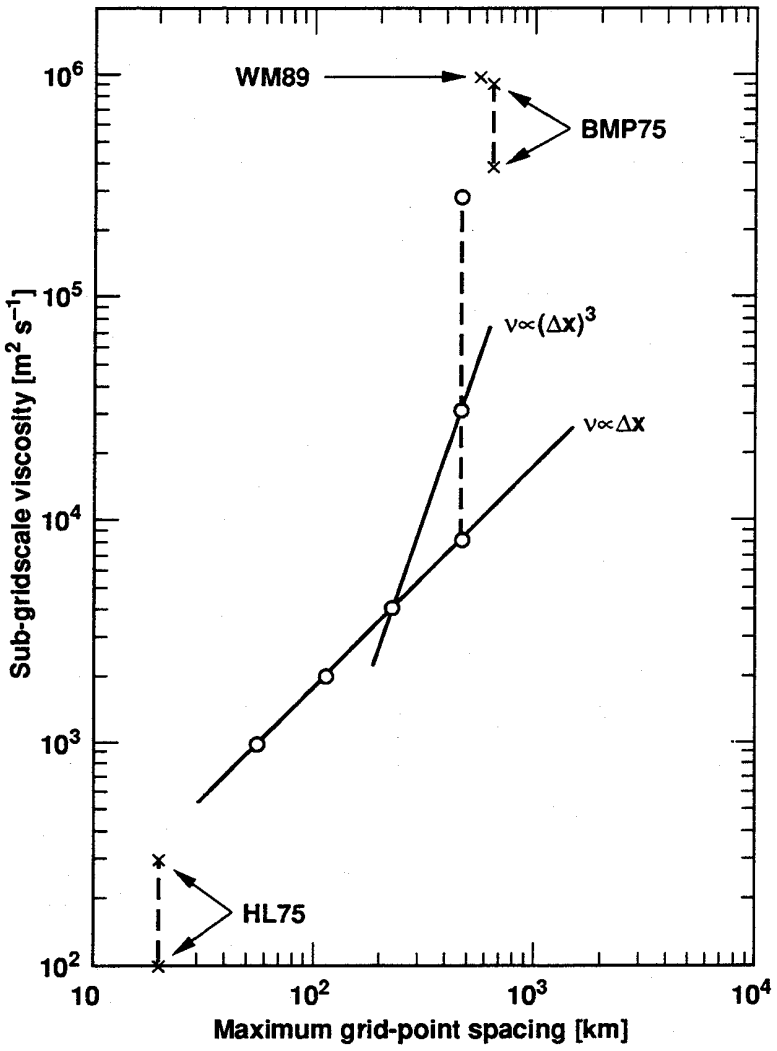

Fig. 1: Horizontal spacing of grid points and horizontal sub-gridscale viscosity coefficients used in this study (circles) and in examples of other OGCM work (crosses). The latter include Holland and Lin (1975a,b; labeled HL75), Bryan et al. (1975; labeled BMP75) and Washington and Meehl (1989; labeled WM89).

spacing (i.e., 8×10^3 m^2 s^{-1}) together with three different choices of momentum diffusion coefficient: scaled linearly to 8×10^3 m^2 s^{-1}, scaled from 2° x 2° roughly as the cube of grid-point spacing (to 3×10^4 m^2 s^{-1}) and, finally, a very large value (3×10^5 m^2 s^{-1}) comparable to coefficients traditionally employed in coarse-resolution global-scale OGCMs. Justification for scaling sub-gridscale diffusion coefficients linearly with grid-point spacing at high resolution and as the cube of grid-point spacing at low resolution is presented by Bryan et al. (1975). In essence the argument is that the minimum acceptable diffusion coefficient is controlled at high resolution by the Reynolds number associated with grid-point spacing, and at low resolution by the need to resolve western boundary currents. Boundary current width, according to scale analysis, is proportional to $(v/ß)^{1/3}$, where v is sub-grid-scale viscosity and ß is the latitude gradient of the Coriolis parameter.

The model is forced by annual mean observed values of sea surface temperature and salinity (Levitus, 1982) and annual mean observed values of surface wind stress (Hellerman and Rosenstein, 1983). Wind stress provides a flux boundary condition on the GCM's momentum conservation equation. Fluxes of heat and salt at the surface are set up to drive surface temperature and salinity toward observations with a relaxation time of one month. Temperature and salinity are similarly constrained at the latitude boundaries of the model, 70°S and 62°N, as an alternative to extending the model to the North Pole and Antarctica and explicitly calculating sea ice behavior and bottom water formation.

3. Spinup

All four resolution runs at LLNL were "spun up" to steady state by the procedure of Semtner and Chervin (1988). In each case the model began with zero current and horizontally uniform temperatures, and with extra Newtonian-relaxation terms in the salinity and thermal energy equations that force salinity and temperature to observed values (Levitus, 1982): so-called robust-diagnostic forcing. This forcing was gradually reduced—"Phase 1 - Phase 3" as described in Semtner and Chervin's Table 1—as spinup proceeded over about twenty years of simulated time. The runs ended with a ten-year integration in which all Newtonian-relaxation terms were dropped above 700 meters depth, below which a three-year-timescale relaxation remained ("free thermocline" run). Most of the spinup was accelerated

by increasing salinity and temperature timesteps by a factor of seven over momentum timesteps (Bryan, 1984). Results described below, however, are from the final year, which was run unaccelerated. Table 1 summarizes the input parameters for the runs.

Figure 2 shows the average of kinetic energy over the entire ocean volume as a function of time for three of the four resolution cases (breaks in some of the curves in Figure 2 occur at boundaries between different phases of spinup as described above). At the end of the integrations the time rate of change of kinetic energy was about 1% or less of the work done by wind stress, showing that the runs attained a steady state. For all but the coarsest of resolutions, kinetic energy decreases as the spacing between grid points is increased, as expected. The exception is that kinetic energy at 2° x 2° resolution is exceeded by kinetic energy at 4° x 4° resolution when sub-gridscale momentum mixing in the latter is set to its lowest value. (As shown below, this anomalous result is a numerical artifact. The highest-momentum-mixing case gave the best of the 4° x 4° resolution simulations, and this case provides the 4° x 4° results discussed below unless otherwise specified.) Note also from Figure 2 that I performed two additional sensitivity tests at 4° x 4° resolution. In these tests the robust-diagnostic forcing was either removed entirely or strengthened and extended to all levels of the model.

The highest resolution case, 1/2° x 1/2°, was spun up at NCAR by Semtner and Chervin, who provided the end of their run as initial conditions for the 1/2° x 1/2° integration at LLNL. The spinup history for this case is not available to me at present, but final values of its kinetic energy are about 0.6 J m^{-3}. Even this value is considerably below that of the actual ocean. Traditional observations, which include mainly the time-mean component of ocean circulation, provide a lower bound of ocean kinetic energy. Peixoto and Oort (1992, Table 13.2) obtain an energy per unit surface area of about 8×10^3 J m^{-2}, i.e., energy per unit volume of about 2 J m^{-3} since the ocean is on average 4 km deep.

4. Circulation snapshots

In this section I describe circulation snapshots from the end points of the integrations shown in Figure 2. For the most part, circulation is depicted by the barotropic transport streamfunction in a horizontal plane. The difference between any

Table 1: Semtner - Chervin Model Runs at LLNL

Title in Fig. 2	Grid Spacing	v_{eddy} [m^2 s^{-1}]	Range of Robust-Diagnostic Forcing	Initial Conditions
(not included in Fig.2)	1/2°	1×10^3	below 700 m	end of S and C's NCAR run
1 deg x 1 deg	1°	2×10^3	below 700 m	isothermal / at rest
2 deg x 2 deg	2°	4×10^3	below 700 m	isothermal / at rest
4 deg x 4 deg	4°	8×10^3	below 700 m	isothermal / at rest
4 x 4 HI-NU	4°	3×10^4	below 700 m	isothermal / at rest
4 x 4 VHN ("very hi nu")	4°	3×10^5	below 700 m	isothermal / at rest
4 x 4 VHN NO FR ("no free thermocline")	4°	3×10^5	everywhere	isothermal / at rest
4 x 4 VHN ALL FR ("all-free thermocline")	4°	3×10^5	nowhere	isothermal / at rest

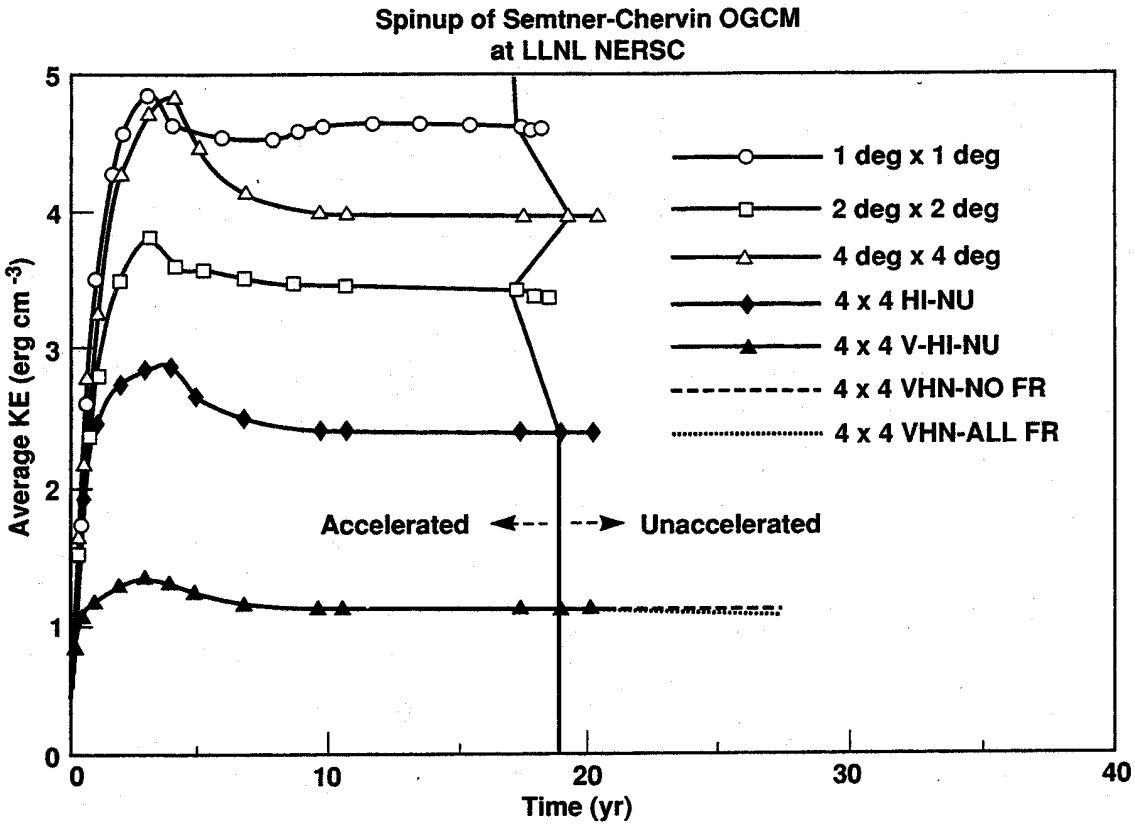

Fig. 2: Integrated kinetic energy as a function of simulated time for spinup of three of the four resolution cases run at LLNL. The dividing line between integrations that were accelerated by the procedure of Bryan (1984) and conventional (unaccelerated) integrations is indicated. Labels indicate which resolution and, in the case of 4° x 4°, distinguish sensitivity tests. See Table 1 for notation.

two isolines of streamfunction gives the vertically integrated volume transport between them, with higher values to the right of the flow direction. The streamfunction is set to zero as a boundary condition along the coasts of North and South America, Africa and Eurasia.

Figure 3 shows a global view of the barotropic streamfunction for the four resolution cases. Present in all cases are subtropical gyre circulations—clockwise in the North Atlantic and North Pacific, counterclockwise in the South Atlantic, South Pacific and southern Indian Ocean—and an eastward-flowing Antarctic Circumpolar Current. The subtropical gyres and the Antarctic Circumpolar Current have long been apparent in observations. Evidently the model's simulation of the largest-scale features of ocean circulation in a horizontal plane is not sensitive to horizontal resolution, except for a strengthening of the Kuroshio and Antarctic Circumpolar Currents as resolution is increased (see also Figure 6).

Figure 4 compares streamfunctions for the different sensitivity tests performed at 4° x 4° resolution. A continuous color variation with streamfunction value is used, instead of constant colors for each of several ranges as in Figure 3. This graphical technique facilitates identification of incipient numerical instability, which appears as oscillations of streamfunction between adjacent grid points—a checkerboard pattern in the images. The two lower-momentum-mixing cases differ from the highest-momentum mixing case (at bottom; same data as in upper left of Figure 3) mainly in the larger amount of two-grid-point oscillations. In other words, the larger kinetic energy values obtained in the lower-mixing cases are an artifact of inappropriately weak sub-gridscale mixing. Essentially no difference is apparent in comparing the end points of 3000-day runs with and without robust-diagnostic forcing. When the Semtner-Chervin model is integrated without robust-diagnostic forcing for a much longer time, however, it shifts to a slightly different thermocline structure (Washington and Meehl, 1992).

Despite the similarity of circulations at the largest scales among the resolution cases, examination in more detail of regional subsets of this information reveals significant differences. For example, Figure 5 shows the barotropic streamfunction in the Gulf Stream region. Even at 4° x 4° resolution the Gulf Stream is recognizable as a narrow current near the east coast of North America. As resolution is increased, however, the current narrows further and a well-defined "recirculation" to the east of the Gulf Stream becomes apparent, bringing the simulation

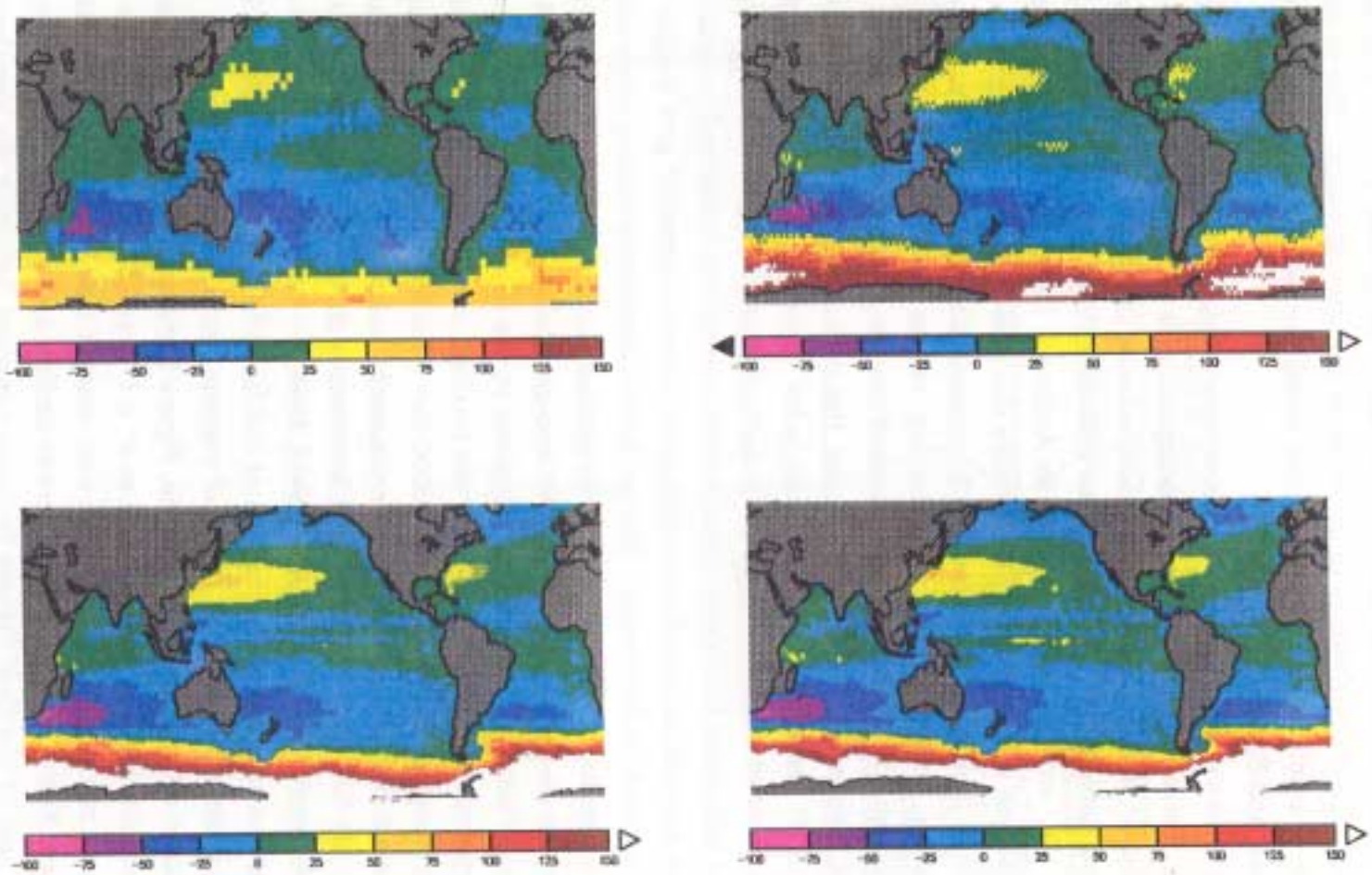

Fig. 3: Barotropic streamfunction values for the four resolution cases: 4° x 4° (upper left), 2° x 2° (upper right), 1° x 1° (lower left) and $1/2^{\circ}$ x $1/2^{\circ}$ (lower right). Colors denote intervals of 25 x 10^{6} m^{3} s^{-1} as indicated in the color bars.

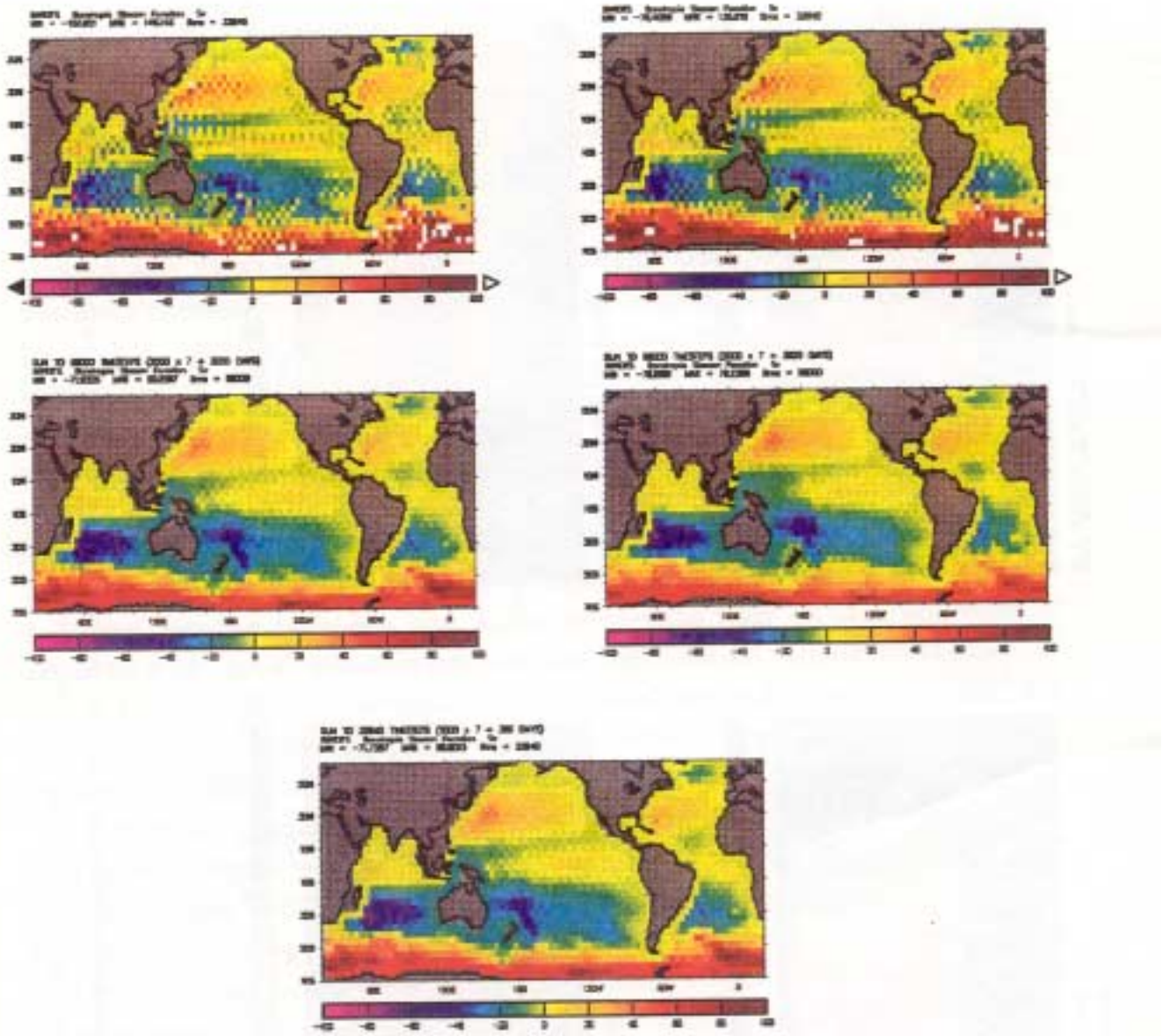

Fig. 4: Barotropic streamfunction values for the 4° x 4° resolution case in sensitivity tests that differ from the "base case" either in sub-gridscale viscosity (upper two panels) or in robust-diagnostic forcing (lower two panels). Sub-gridscale viscosity is 8×10^3 m^2 s^{-1} in the upper left, 3×10^4 m^2 s^{-1} in the upper right and 3×10^5 m^2 s^{-1} in the remaining panels. The two middle panels show runs extended by 3000 days simulated time (see Figure 1) in which robust-diagnostic forcing is either present with a one-year relaxation time everywhere (middle left) or absent everywhere (middle right). The bottom panel shows the "base case" itself, i.e., the same data shown in the upper left of Fig. 3.

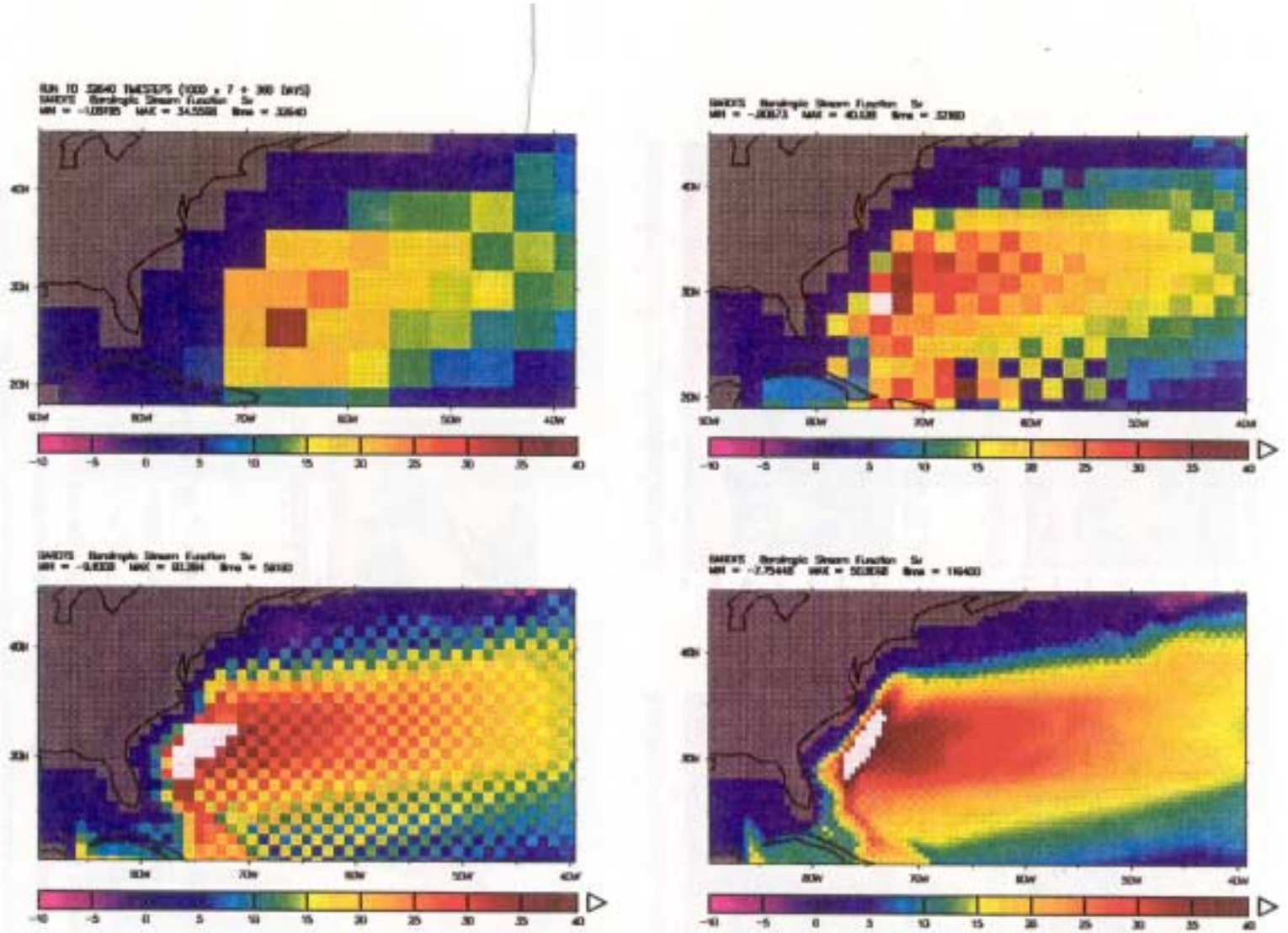

Fig. 5: Barotropic streamfunction values in the Gulf Stream region for the four resolution cases: 4° x 4° (upper left), 2° x 2° (upper right), 1° x 1° (lower left) and $1/2^{\circ}$ x $1/2^{\circ}$ (lower right).

into better agreement with observations. Western boundary currents not shown in Figure 5 also exhibit qualitative improvement as resolution is increased. The simulated Aghulas Current penetrates from the Indian Ocean into the South Atlantic, and the simulated East Australian Current becomes better defined, though its volume transport remains below observations. The larger-scale Kuroshio Current off Japan, however, intensifies to a value comparable with observations as resolution is increased, as shown in Figure 3 and below.

Quantitative elements of comparison between an ocean model's simulated circulation and observations are provided by volume transports in narrow western boundary currents or through straits. Figure 6 shows the model-simulated transports as a function of resolution. Simulated flow through the Drake Passage between South America and Antarctica intensifies with increasing resolution and appears to asymptote near 200 x 10^6 m^3 s^{-1}, a value considerably exceeding observations (120 x 10^6 m^3 s^{-1}; see Whitworth and Peterson, 1985). Flow in the Kuroshio strengthens with increasing resolution to approximately its observed value (Masuzawa, 1972, Fig. 2), but flow in the Gulf Stream remains below its observed value (Stommel, 1965, Fig. 6) for all resolutions studied. Finally, southwestward transport between Indonesia and Australia remains near its observed value of about 20 x 10^6 m^3 s^{-1} (Godfrey and Golding, 1981) for all resolutions studied. It should be noted that the foregoing "observations" are highly uncertain; they are derived in large part from sparse measurements of temperature and salinity together with the assumption of geostrophic balances.

Additional information about the solutions' resolution dependence is revealed by simulated temperatures. For example, Figure 7 shows the temperature field near the surface in the Eastern Pacific. Large-scale patterns are identical for the four resolutions, not a surprising result considering the upper boundary condition that forces surface temperatures toward agreement with observations. The figure, however, reveals subtropical waves west of South America in the 1° x 1° and 1/2° x 1/2° cases. (These waves, also present east of Africa, appear in careful examination of the barotropic streamfunction shown in Figure 3.) Animation of the 1/2° x 1/2° simulation shows that the waves propagate westward with about the same speed as the local current, about 0.1 m s^{-1}. Since their wavelength is ~1000 km, their period is ~10^7s or a little over 100 days. These waves do not seem identifiable with familiar theoretical types like Kelvin or Rossby waves. Nevertheless the simulated

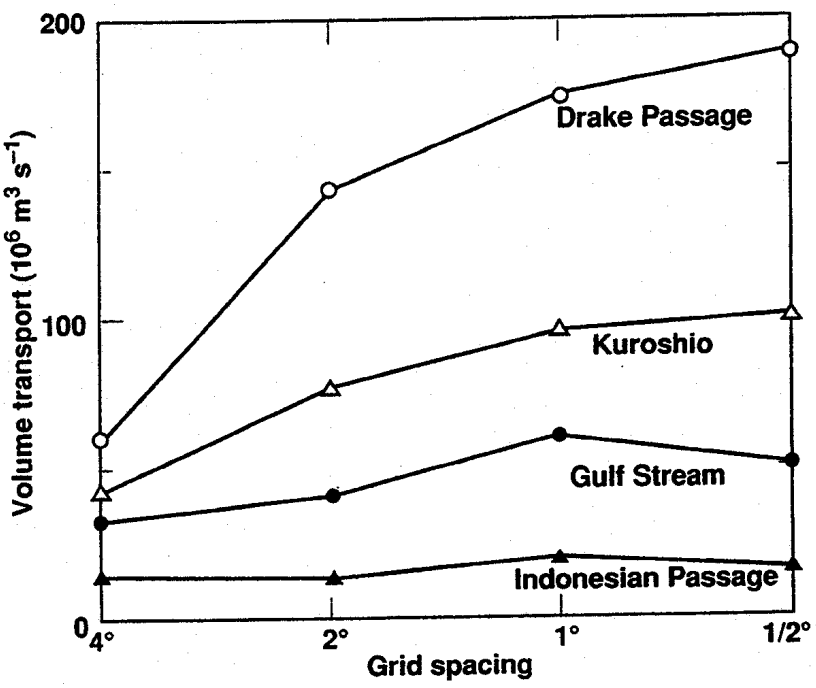

Fig. 6: Volume transports through indicated straits and western boundary currents as a function of horizontal grid-point spacing.

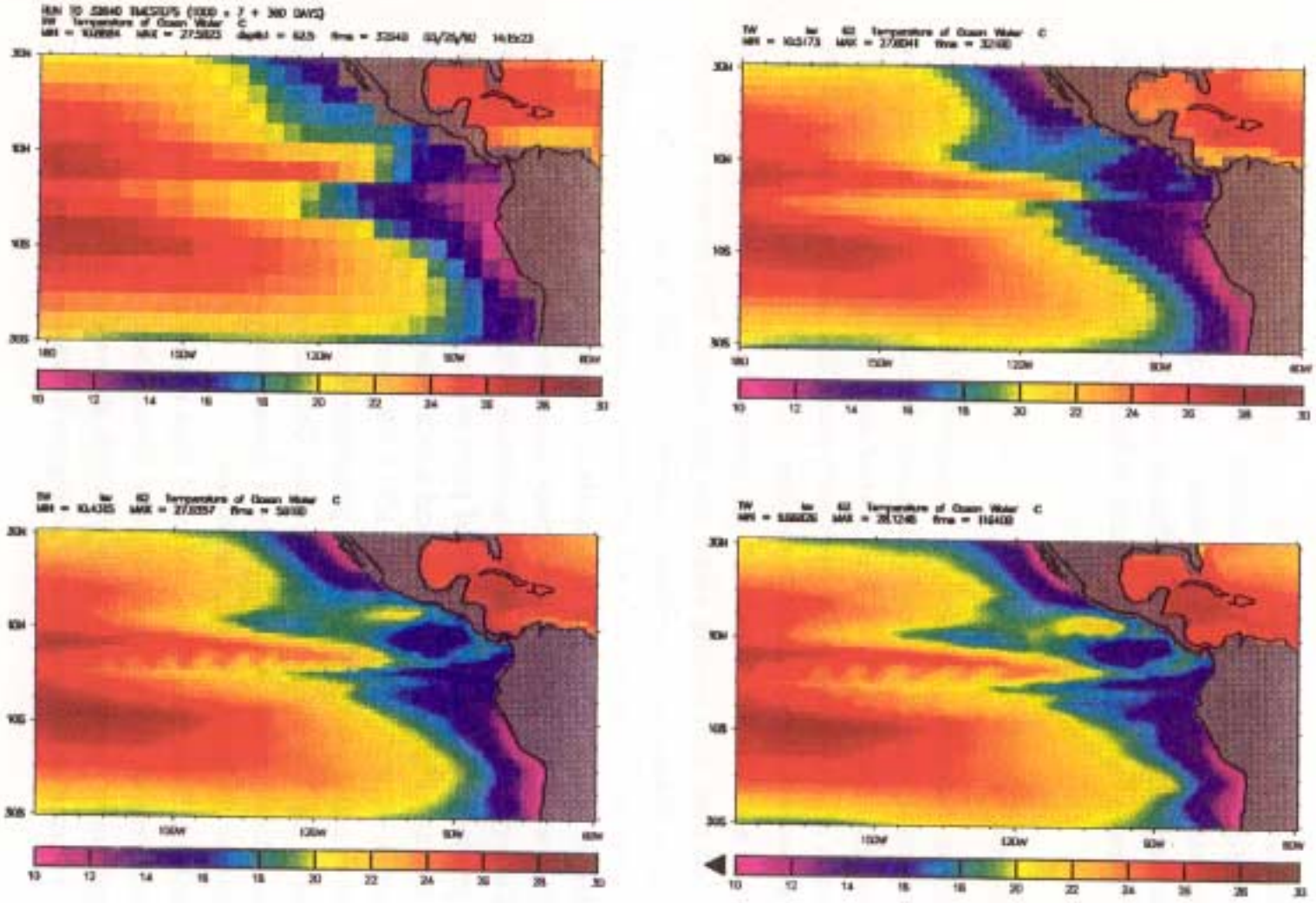

Fig. 7: Eastern Pacific temperatures in model's third layer from the top (62 meters depth) for the four resolution cases: 4° x 4° (upper left), 2° x 2° (upper right), 1° x 1° (lower left) and 1/2° x 1/2° (lower right).

waves resemble certain waves appearing in observations of ocean temperature and kinetic energy (Peixoto and Oort, 1992, Sec. 8.5).

Except for the waves discussed above, no significant time variations are apparent in the circulation of any of the resolution cases. In particular there is no evidence of mesoscale eddies. These eddies begin to emerge in the 1/2° x 1/2° simulation when the Laplacian sub-gridscale diffusion used here is replaced by a more scale-selective parameterization, biharmonic diffusion (Semtner and Chervin, 1988).

5. Heat transport

In this section I describe the ocean's transport of heat from the relatively warm tropics to cooler middle and high latitudes. Results for this section were obtained from output statistics of the last year of each model run (see Figure 2). Actually the length of time averaging is irrelevant since, as mentioned above, there is virtually no time-varying component to the flow.

As simulated by a GCM, poleward heat transport comes in two varieties: explicitly advected heat, and mixing below the grid scale. The former is proportional to the product of simulated northward current velocity v and temperature T; the latter is determined by the model's sub-gridscale parameterizations. As noted above, sub-gridscale mixing of heat in this study is accomplished by simple downgradient diffusion with the diffusion coefficient linear in grid spacing. Figure 8 shows the total of explicit advection and sub-gridscale diffusion for the four resolution cases. To produce these one-dimensional plots as functions of latitude, northward heat flux is integrated over longitude and depth. Also shown in the figure are results from Barton's (1988) analysis of the 1/2° x 1/2° resolution version of Semtner and Chervin's model with sub-gridscale parameterizations and boundary conditions identical to my 1/2° x 1/2° resolution run. Comparison of Barton's and my results provides a measure of the uncertainty of these values due to slightly different initial conditions and postprocessing methods.

In the Southern Hemisphere the poleward heat transport decreases steadily as resolution is increased, while in the Northern Hemisphere the heat transport is relatively insensitive to resolution. Figure 9, which shows only the diffusion component of heat transport on the same scale as Figure 8, makes it clear that most of

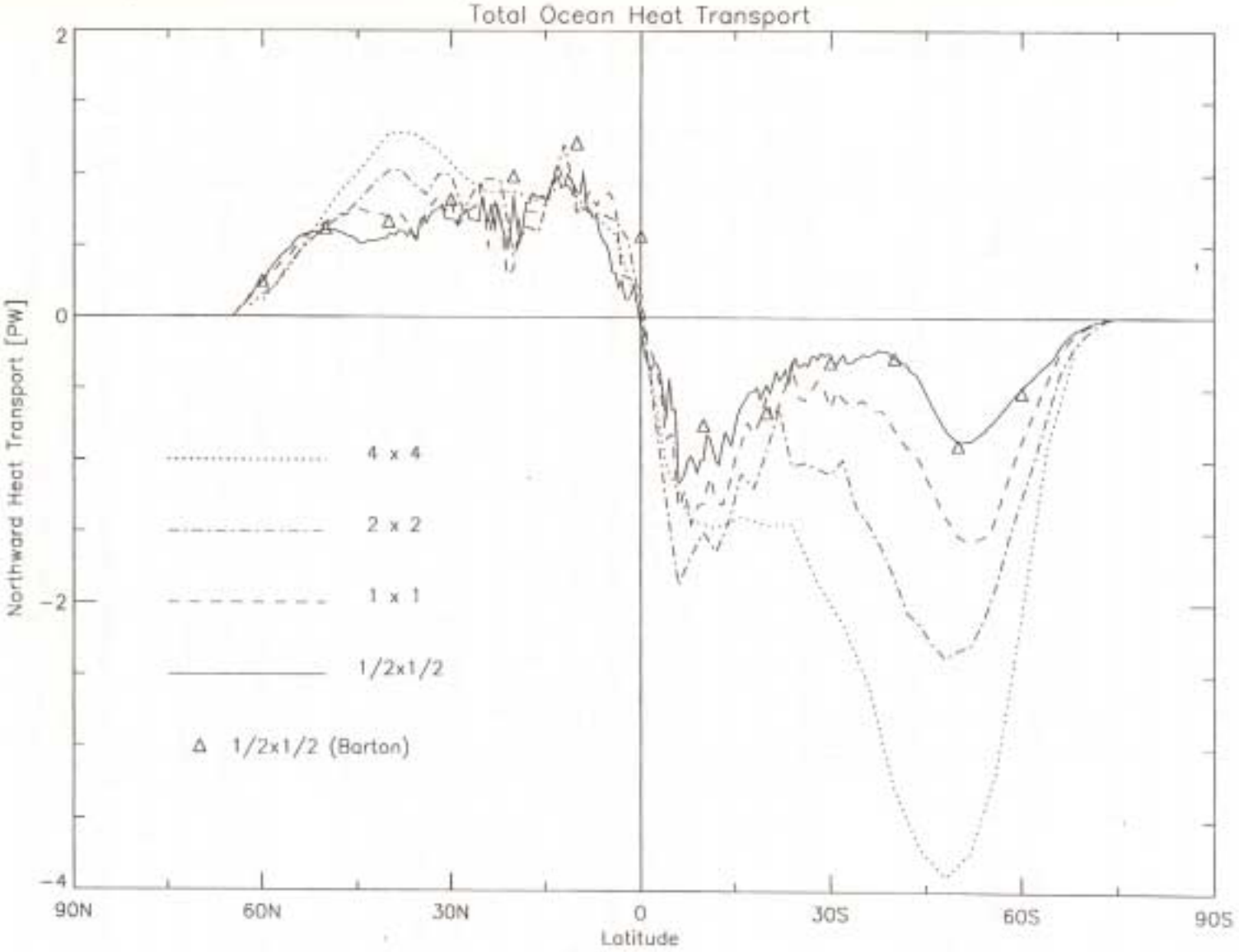

Fig. 8: Total ocean heat transport, integrated over longitude and depth, for the four resolution cases as a function of latitude. Also shown is Barton's (1988) independent analysis of the 1/2° x 1/2° Laplacian-diffusion version of the model.

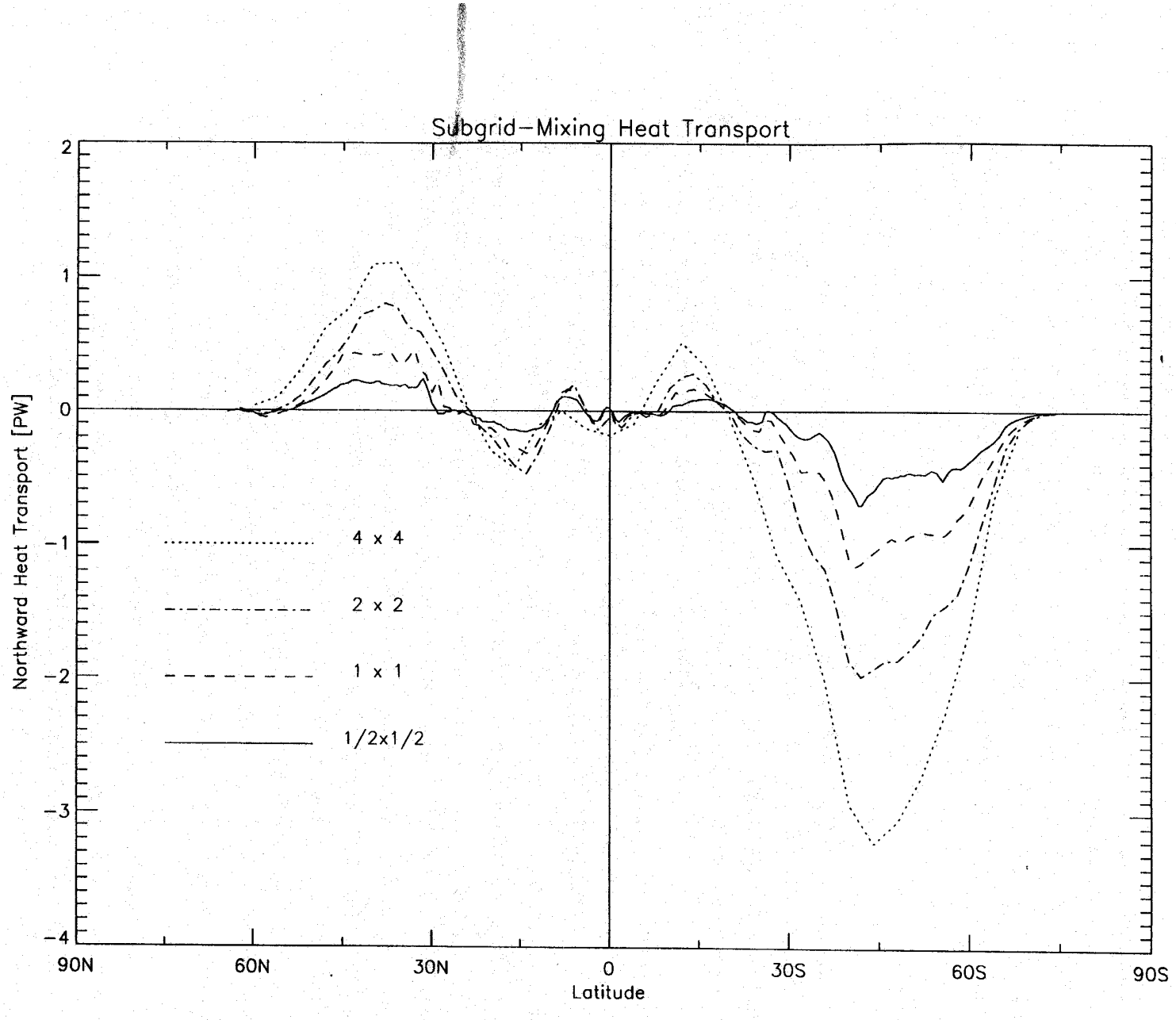

Fig. 9: Sub-gridscale diffusion component of ocean heat transport, integrated over longitude and depth, for the four resolution cases as a function of latitude.

this sensitivity arises from the diffusion component. In fact, for resolutions coarser than 1° x 1° most of the simulated ocean heat transport is due to sub-gridscale diffusion. Diffusive heat transport is strongly linked to resolution because the equator-to-pole distribution of ocean temperature is relatively insensitive to resolution, while the coefficient of diffusive transport is linear in grid spacing. At 1/2° x 1/2° resolution, the diffusion component is less than half the total heat transport, except in the Southern Hemisphere's middle latitudes.

The explicit-advection part of simulated heat transport can be subdivided into components arising from the time-average (denoted by an overbar), deviation from the time-average (denoted by a prime), the longitude-average (denoted by square brackets) and deviation from the longitude-average (denoted by an asterisk):

$$[\overline{vT}] = [\bar{v}]\,[\bar{T}] + [\bar{v}^{*}\bar{T}^{*}] + [\overline{v'T'}] \qquad (1)$$

The first term on the right side of (1) arises from steady-state overturning in a meridional plane, i.e., warm water flowing poleward at the surface while cooler water flows equatorward at depth. The contribution to ocean heat transport from this term is shown in Figure 10. The second term on the right side of (1) arises from the so-called gyre circulation, in which warm water flows poleward on the western sides of ocean basins (e.g., in the Gulf Stream) while cooler water flows equatorward elsewhere. This term's contribution to ocean heat transport is shown in Figure 11. The final term on the right of (1) arises from time-dependent eddies, predominantly mesoscale eddies in large-scale ocean GCMs. (An additional contribution to the final term, $\overline{[v]'[T]'}$, arises from time-dependent meridional overturning, but this is probably negligible in all cases discussed here, which are generated with annual mean boundary forcings.) The time-dependent final term in (1) is negligible for all cases discussed here except for the biharmonic-diffusion run, which resolves a significant number of mesoscale eddies.

Comparison of Figures 10 and 11 shows that most of the simulated explicit-advection heat transport is due to meridional overturning (note the change in scale between the two figures). The meridional overturning component is poleward except in the middle latitudes of the Southern Hemisphere, where the transport becomes equatorward when resolution is made greater than 4° x 4°. This exception is consistent with observations of a thermally indirect wind-driven "Deacon circulation" at these latitudes (see, e.g., Bryan et al., 1988). The gyre component is pole-

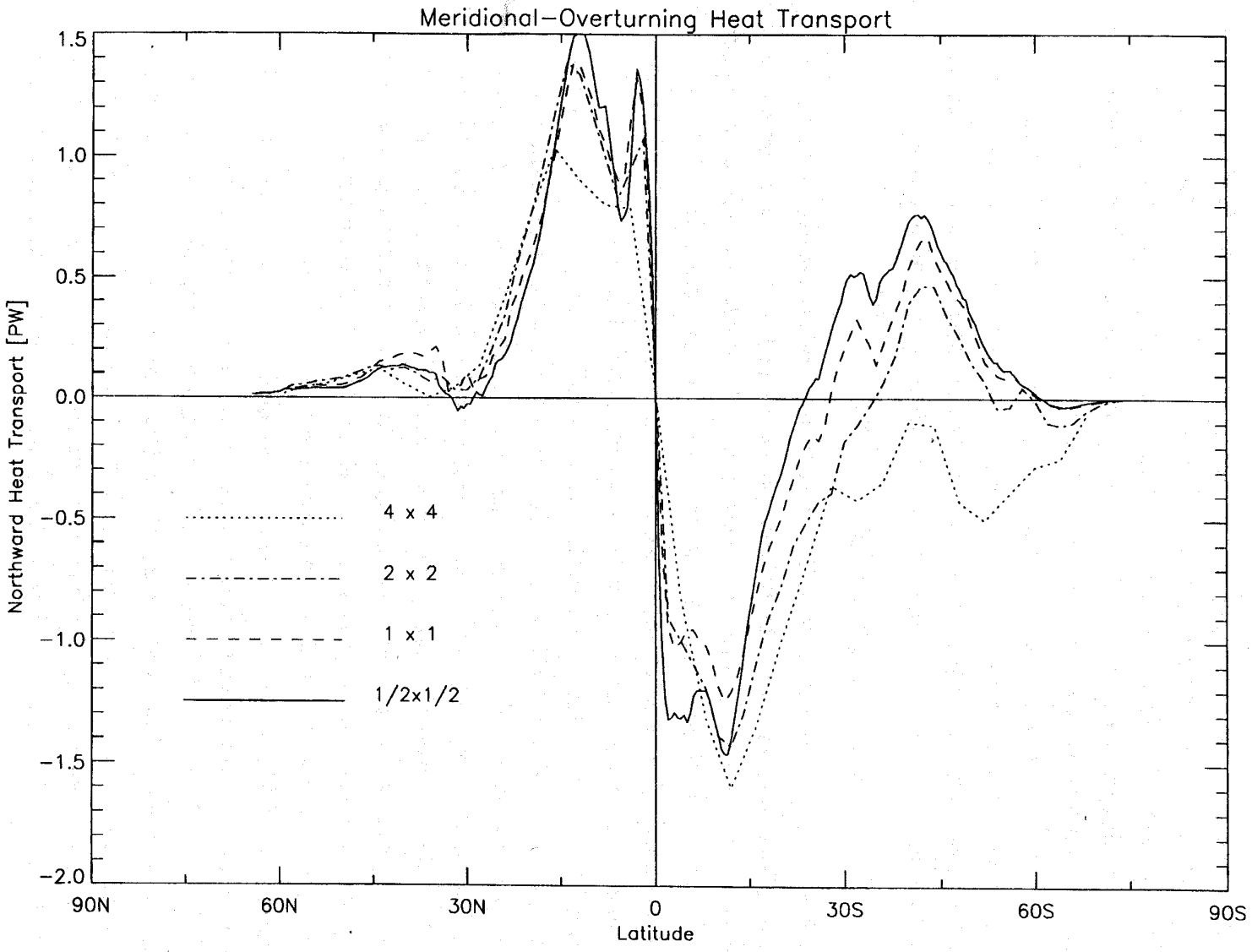

Fig. 10: Meridional overturning component of ocean heat transport, integrated over longitude and depth, for the four resolution cases as a function of latitude.

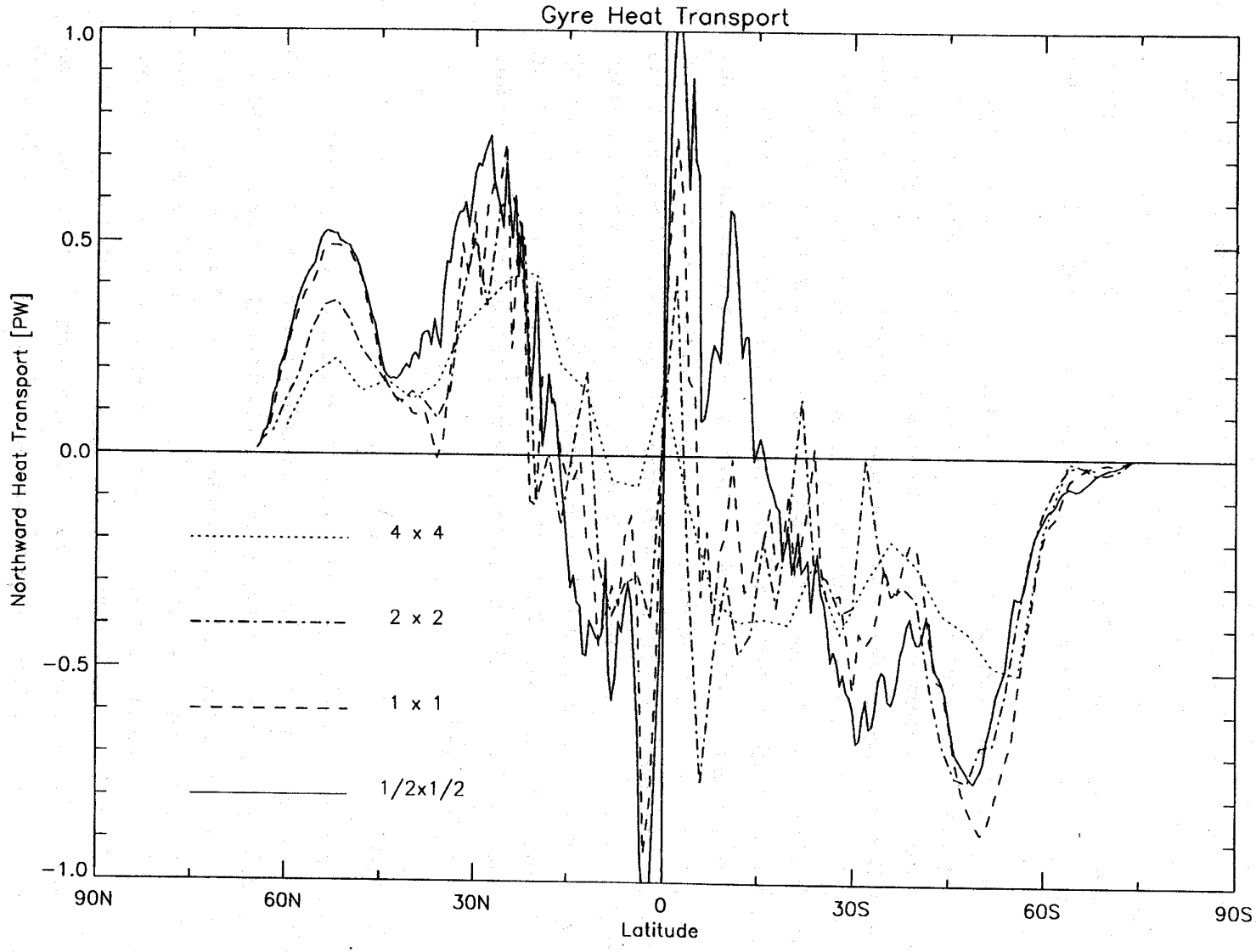

Fig. 11: Gyre component of ocean heat transport, integrated over longitude and depth, for the four resolution cases as a function of latitude.

ward at middle and high latitudes but equatorward near the Equator. Both components of explicit-advection heat transport show some increase in magnitude with increasing resolution, but the increase is small compared with the corresponding decrease in sub-gridscale diffusion. Thus the magnitude of total heat transport (Figure 8) generally decreases with increasing resolution—although as mentioned previously it appears to converge to a peak value of about 1 PW in the Northern Hemisphere.

The peak values of ocean heat transport simulated here are significantly below their observed counterparts. Figure 12 shows total simulated ocean heat transport (same as in Figure 8) together with values inferred from observations using two different methods. Both methods involve integrating the annual mean energy flux into or out of the sea surface to obtain total poleward heat transport by the ocean. Hastenrath (1982) uses sea surface fluxes that are more or less directly measured, while Carissimo, Oort and Vonder Haar (1985) infer sea surface fluxes indirectly from top-of-atmosphere energy fluxes measured from satellites and atmospheric energy transport inferred from weather balloon data. I've argued elsewhere that the latter method underestimates atmospheric heat transport and thus overestimates ocean heat transport (Covey, 1988). Even the ocean heat transport obtained by the former method, however, is about a factor of two greater than the model-simulated transport. This problem is typical of global ocean GCMs. In the following section I address the question of whether the problem is due to failure to resolve mesoscale eddies.

6. Conclusions

Several "caveats" apply to the results summarized above. First, Semtner and Chervin's model has never before been run at a resolution as coarse as 4° x 4°. The 4° x 4° results presented here could be improved by additional "tuning" of sub-gridscale parameterizations, beyond the adjustment of momentum mixing discussed above. For example, Meehl et al. (1982) obtain from a 5° x 5° ocean GCM the same unrealistically large magnitude of poleward heat transport in the Southern Hemisphere as in the 4° x 4° case presented here. Meehl et al. show that their heat transport can be reduced to more reasonable values, however, by simply decreasing the coefficient of Laplacian sub-gridscale heat mixing from 2×10^4 m^2 s^{-1} to 2×10^3

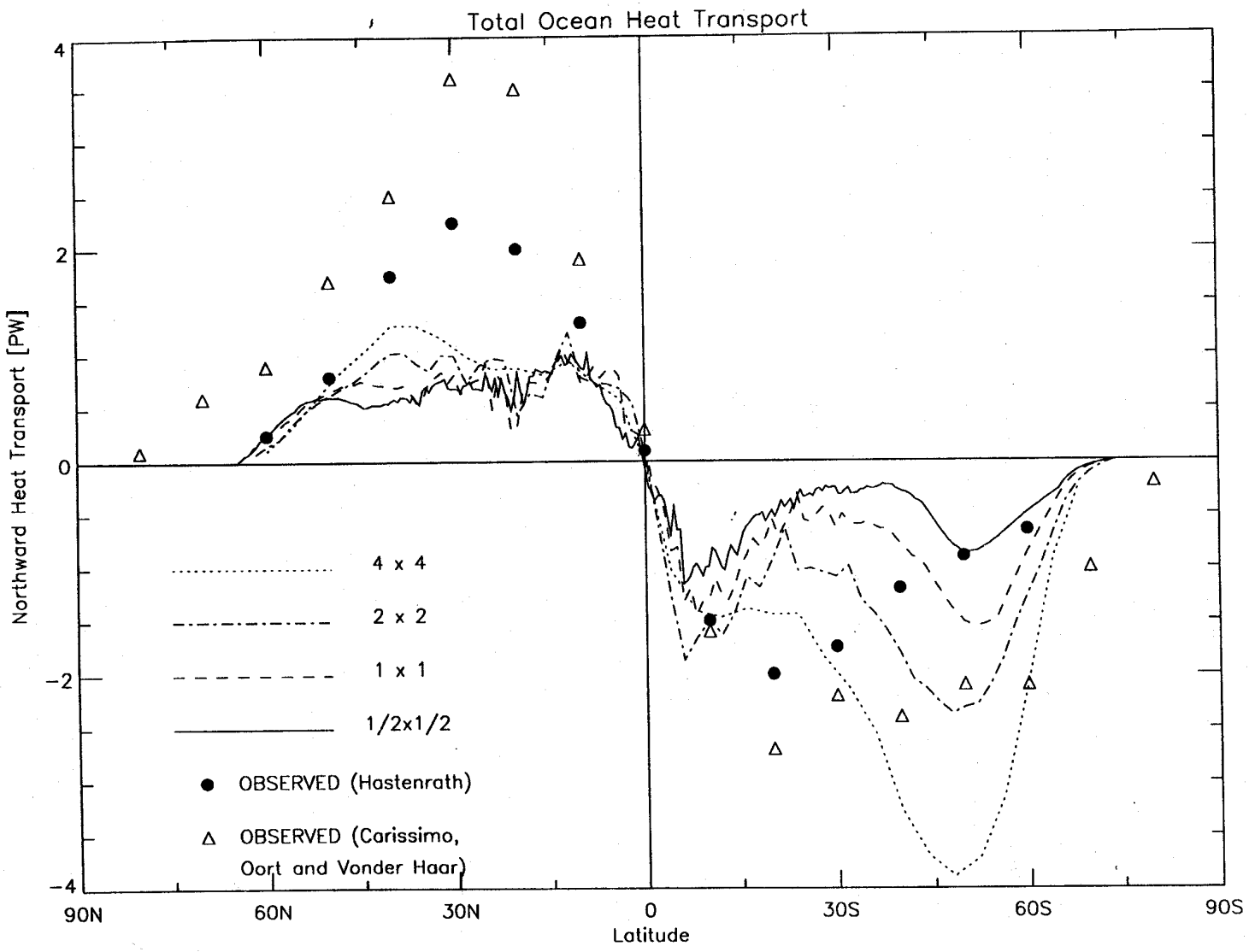

Fig. 12: Total ocean heat transport, integrated over longitude and depth, for the four resolution cases as a function of latitude. Also shown are values inferred from observations by Hastenrath (1982) and Carissimo et al. (1985).

$m^2\ s^{-1}$ without changing model resolution. (Recall that the coefficient used in the 4° x 4° results presented here is $8 \times 10^3\ m^2\ s^{-1}$.) Another parameter that might be tuned is bottom topography. Widening the Drake Passage, for example, might allow a more realistic (i.e., larger) Antarctic Circumpolar Current in the 4° x 4° case. Considerations such as these imply that modeling the global ocean at about 4° x 4° resolution may not be as bad as it looks in this report, and that the differences among the different resolution cases need not be as great as presented here.

On the other hand, differences among the four resolution cases are artificially minimized by several constraints. First, as mentioned above, the deep ocean in all cases is pushed toward observed values of temperature and salinity by nonphysical Newtonian relaxation terms added to the conservation equations for heat and salt below 700 meters depth. Second—and in my opinion more important—the model's boundary condition essentially pins temperature and salinity to observations at the sea surface. Temperature and salinity are similarly fixed at the latitude boundaries of the model, instead of extending the model to the North Pole and Antarctica and explicitly calculating sea ice behavior. By thus constraining temperature and salinity, the model places restrictions on how much the geostrophic component of circulation can vary among the different resolution cases.

Nevertheless I find the large-scale thermal structure and circulation remarkably similar among the 1/2° x 1/2°, 1° x 1° and 2° x 2° resolution cases. The 4° x 4° case, in contrast, appears to be an "outlier" incapable of resolving narrow western boundary currents (Figure 5) and often severely underestimating the strength of the observed circulation (Figure 6). Similarly, ocean heat transport simulated by the four cases in the Northern Hemisphere converges to consistent if disturbingly low values as grid spacing is reduced below 4°. In the Southern Hemisphere convergence is not apparent, due to the dominance of sub-gridscale heat diffusion at most resolutions, but this result may well be an artifact of overly large heat diffusion coefficients.

There remains the issue of mesoscale eddies. As noted above, mesoscale eddies are absent even at 1/2° x 1/2° resolution unless the Laplacian diffusion of heat and momentum is replaced by a more scale-selective parameterization. Doing so, Semtner and Chervin (1988) find considerable eddy activity in their simulation. Figure 13, taken from unpublished results of Semtner and Chervin, shows the corresponding ocean heat transport. (The heat transport shown in Figure 3 of Semt-

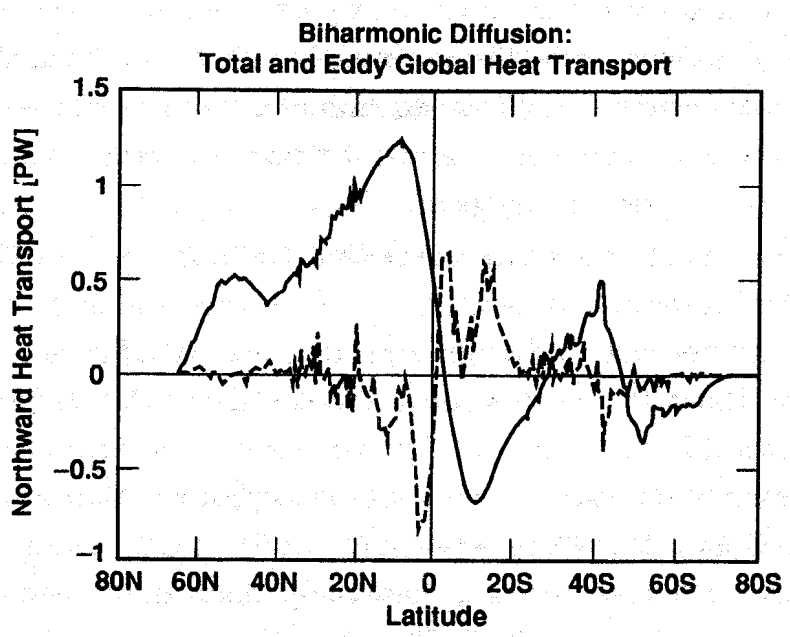

Fig. 13: Ocean heat transport due to the mean flow (solid line) and due to eddies (dashed line), integrated over longitude and depth, for 1/2° x 1/2° with biharmonic diffusion of momentum (see Semtner and Chervin, 1988, for diffusion coefficient values and discussion of the circulation).

ner and Chervin (1988) is for the Laplacian-diffusion case, i.e., the same as the 1/2° x 1/2° resolution case presented here. Heat transport for the biharmonic-diffusion case under seasonal cycle forcing is shown by Semtner and Chervin (1992), but the results presented both above and in Figure 13 are for annual mean forcing.) The solid line shows the total contribution of the mean flow—corresponding to the grand total of heat transport in the cases presented above—while the dashed line shows the contribution of eddies, i.e., the final term in Equation 1. It is apparent from the figure that mesoscale eddy heat transport tends to oppose that arising from the mean flow, in agreement with the simplified GCM results summarized by Bryan (1991). It is also evident that introduction of mesoscale eddies has not significantly changed the peak value of ocean heat transport from slightly over 10^{15} W, its value in the non-eddy-resolving case.

In short, the results of this study imply that there is much to be gained by making the horizontal resolution of ocean GCMs finer than the 4°-5° grid spacings used in traditional climate models, but diminishing returns set in as grid spacings are decreased below about 1°. At this point, the simulated circulation (Figure 6) and associated poleward heat transport (Figure 8) seem to be approaching asymptotic limits. Resolution of mesoscale eddies does not appear to significantly change total ocean heat transport; it is worth repeating that this result holds even in (limited-domain) models with resolutions considerably finer than that attained by Semtner and Chervin (see Bryan, 1991). The main "loose end" in the story, in my view, is the substantial disagreement between heat transport simulated in models and heat transport inferred from observations. A good deal of work in both modeling and data analysis may be required to clear up this mystery.

Acknowledgements. It is a pleasure to thank the many individuals whose efforts were essential for initiation and completion of this work. W. Lawrence Gates originally suggested this study. Albert J. Semtner, Jr., and Robert M. Chervin generously contributed not only their model but also a great deal of their time advising on the running of the model on our computer system. Lisa Corsetti reprogrammed the code for execution at LLNL and developed statistical postprocessing software. Finally, John Stout nursed the longer numerical experiments through the local supercomputer network, and Dean N. Williams developed graphics software.

This work was performed under auspices of the U.S. Department of Energy Environmental Sciences Division at the Lawrence Livermore National Laboratory under Contract W-7405-ENG-48.

REFERENCES

Barton, W.A., 1988: *An Analysis or Results of a High-Resolution World Ocean Circulation Model.* M.S. thesis, Naval Postgraduate School, Monterey, CA, 146 pp.

Bryan, K., S. Manabe and R.K. Pacanowski, 1975: A global ocean-atmosphere climate model. Part II. The oceanic circulation. *J. Phys. Oceanogr.*, **5**, 30-46.

Bryan, K., 1984: Accelerating the convergence to equilibrium of ocean-climate models. *J. Phys. Oceanogr.*, **14**, 666-673.

Bryan, K., 1986: Poleward bouyancy transport in the ocean and mesoscale eddies. *J. Phys. Oceanogr.*, **16**, 927-933.

Bryan, K., S. Manabe and M.J. Spelman, 1988: Interhemispheric asymmetry in the transient response of a coupled ocean-atmosphere model to a CO2 forcing. *J. Phys. Oceanogr.*, **18**, 851-867.

Bryan, K., 1991: Poleward heat transport in the ocean. Tellus, 43AB, 104-115.

Carissimo, B.C., A.H. Oort and T.H. Vonder Haar, 1985: Estimating the meridional energy transports in the atmosphere and ocean. *J. Phys. Oceanogr.*, **15**, 82-91.

Covey, C., 1988: Atmospheric and oceanic heat transport: simulations versus observations. *Climatic Change*, **13**, 149-159.

Gates, W.L., J.S. Boyle, L.C. Corsetti, C. Covey, P.J. Gleckler, T.J. Phillips, G.L. Potter, K.R. Sperber, and K.E. Taylor, 1992: The effects of horizontal resolution on the seasonal mean climate simulated with the ECMWF model (in preparation).

Godfrey, J.S. and T.J. Golding, 1981: The Sverdrup relation in the Indian Ocean, and the effect of Pacific-Indian Ocean throughflow on Indian Ocean circulation and on the East Australian Current. *J. Phys. Oceanogr.*, **11**, 771-779.

Hastenrath, S., 1982: On meridional heat transports in the World Ocean. *J. Phys. Oceanogr.*, **12**, 922-927.

Hellerman, S., and M. Rosenstein, 1983: Normal monthly wind stress over the world ocean with error estimates. *J. Phys. Oceanogr.*, **13**, 1093-1104.

Holland, W.R., and L.B. Lin, 1975a: On the generation of mesoscale eddies and their contribution to the oceanic general circulation. I. A preliminary numerical experiment. *J. Phys. Oceanogr.*, **5**, 642-657.

Holland, W.R., and L.B. Lin, 1975b: On the generation of mesoscale eddies and their contribution to the oceanic general circulation. II. A parameter study. *J. Phys. Oceanogr.*, **5**, 658-669.

Levitus, S., 1982: Climatological Atlas of the World Ocean. NOAA Professional Paper 13, U.S. Department of Commerce, Rockville, MD, 173 pp.

Manabe, S., K. Bryan and M.J. Spelman, 1990: Transient response of a global ocean-atmosphere model to a doubling of atmospheric carbon dioxide. *J. Phys. Oceanogr.*, **20**, 722-749.

Masuzawa, J. 1972: Water Characteristics of the North Pacific Central Region in *Kuroshio: Physical Aspects of the Japan Current,* H. Stommel and K. Toshida, eds., Univ. Washington Press, Seattle, 517 pp.

Meehl, G.A., W.M. Washington and A.J. Semtner, Jr., 1982: Experiments with a global ocean model driven by observed atmospheric forcing. *J. Phys. Oceanogr.*, **12**, 301-312.

Peixoto, J.P., and A.H. Oort: Physics of Climate. American Institute of Physics, New York, NY, 520 pp.

Semtner, A.J., Jr., and R.M. Chervin, 1988: A simulation of the global ocean circulation with resolved eddies. *J. Geophys. Res.*, **93**, 15502-15522.

Semtner, A.J., Jr., and R.M. Chervin, 1992: Ocean general circulation from a global eddy-resolving model. *J. Geophys. Res.*, **97**, 5493-5550.

Stommel, H., 1965: *The Gulf Stream: A Physical and Dynamical Description*, 2nd Ed., Univ. of Calif. Press, Berkeley, CA, 248 pp.

Washington, W.M., and G.A. Meehl, 1989: Climate sensitivity due to increased CO2: experiments with a coupled atmosphere and ocean general circulation model. *Climate Dynamics*, **4**, 1-38.

Washington, W.M., G.A. Meehl, L. VerPlank and T.W. Bettge, 1992: A world ocean for greenhouse sensitivity studies: Regional intercomparison of two resolutions (0.5° and 1°) and the role of diagnostic forcing. *Climate Dynamics*, in press.

Whitworth, T., III, and R.G. Peterson, 1985: Volume transport of the Antarctic Circumpolar Current from bottom pressure measurements. *J. Phys. Oceanogr.*, **15**, 810-816.

Woods, J.D., 1985: The World Ocean Circulation Experiment. *Nature*, **314**, 501-511.